Available online at www.sciencedirect.com
SCIENCE DIRECT
Polymer 47 (2006) 1630–1639
polymer
www.elsevier.com/locate/polymer

Crystallization behavior of polymer/montmorillonite nanocomposites. Part III. Polyamide-6/montmorillonite nanocomposites, influence of matrix molecular weight, and of montmorillonite type and concentration

Douwe S. Homminga, Bart Goderis, Vincent B.F. Mathot, Gabriel Groeninckx *

Division of Molecular and Nanomaterials, Laboratory of Macromolecular Structural Chemistry, Department of Chemistry, Catholic University of Leuven (KULeuven), Celestijnenlaan 200F, 3000 Heverlee, Belgium

Received 25 March 2005; received in revised form 11 August 2005; accepted 29 October 2005
Available online 17 November 2005

Abstract

Several series of polyamide-6 (PA-6) nanocomposites, differing in montmorillonite (MMT) type and content and PA-6 matrix molecular weight, were prepared by melt-extrusion and the associated PA-6 crystallization behavior and morphology was evaluated using (synchrotron) X-ray diffraction, transmission electron microscopy and differential scanning calorimetry. The nucleating ability of silicate layers is poor in PA-6 nanocomposites made by melt-extrusion because highly active, stable PA-6 crystallization precursors are generated during melt-extrusion. In most of the studied PA-6/MMT nanocomposites the dispersed silicate layers act as impurities and decrease rather than increase the overall crystallization kinetics of PA-6, especially at high MMT contents. Furthermore, at a given MMT concentration, the crystal growth retardation inflates with increasing degree of exfoliation, which dependents on the MMT type and which increases with increasing PA-6 molecular weight. One of the considered MMT types leads to a poorly exfoliated nanomorphology and as a result no retardation of crystal growth is observed. Furthermore, the disturbed crystal growth does not alter the PA-6 semicrystalline stack morphology. Moderate nucleation effects due to the presence of MMT can be observed when the particle load is low (low amount of MMT and/or poor degree of exfoliation) and provided the supercooling is sufficiently large.

Keywords: Polyamides; Nanocomposite; Extrusion

1. Introduction

Polymer-layered silicate nanocomposites (PLSN) display enhanced solid-state material properties such as strength, elasticity modulus, gas barrier resistance and heat distortion temperature compared to the pure polymers [1–7]. These improvements are readily reached with silicate contents as low as 1–4 vol%.

Silicate type minerals, like talc and mica, are well-known nucleating agents for crystallizable polymers [8,9]. It is thus reasonable to expect that nano-sized silicate layers too function as nucleating agents in PLSN. Indeed, an enhanced crystallization rate has recently been reported in the literature [3,6,10–20].

The crystallization behavior of polyamide-6 (PA-6)/montmorillonite (MMT) nanocomposites and the role of the silicate layers has been addressed as well [3,6,10,11,14–17,19]. Such studies are very complicated due to the unusual crystallization behavior of the neat PA-6 itself. First of all, crystalline PA-6 displays different polymorphic structures, in particular the monoclinic α- and the pseudohexagonal γ-forms, and their relative amounts are influenced by the presence of silicate layers [3,11,12,14–17]. Secondly, during thermal characterization several phase transitions ($\alpha \rightarrow \gamma$, Brill transition), besides simple melting, have to be considered in, e.g. a differential scanning calorimetry (DSC) heating run [3,12,15].

An interesting phenomenon that has been observed in extruded PA-6/MMT nanocomposites is that besides the nucleating effect, the silicate layers can also clearly retard the crystal growth process [10,21]. After a small initial increase in overall crystallization rate at low MMT concentrations, the dispersed silicate layers decrease the overall PA-6 crystallization rate with further increase of the MMT content. At these higher concentrations, the silicate layers behave as heterogeneities that retard the PA-6 crystal growth, rather than acting

* Corresponding author. Tel.: +32 16 327440; fax: +32 16 327990.
E-mail address: gabriel.groeninckx@chem.kuleuven.ac.be (G. Groeninckx).

0032-3861/$ - see front matter © 2006 Elsevier Ltd. All rights reserved.
doi:10.1016/j.polymer.2005.10.141

as nucleating agents. This phenomenon is hardly observed in PA-6 nanocomposites prepared by in situ polymerization on the account of the strong influence of processing conditions on the crystallization behavior of PA-6. The crystallization temperature of PA-6 increases about 15 °C after melt-extrusion. It has been suggested that the partly oriented segments of polymer chains that are generated during extrusion are transformed into efficient nucleating agents upon cooling. Moreover, these structures turn out to be quite stable because the original (virgin) state cannot be restored by temperature cycling [10,22–25]. Therefore, the role of silicate layers as nucleating agents is much more pronounced in PA-6 nanocomposites that have not been prepared by melt-extrusion because the extrusion induced stable structures that function as nucleating agents are not present in these nanocomposites and therefore cannot overrule the silicate layer induced nucleation.

A highly important parameter for the crystallization behavior of PA-6/MMT nanocomposites is the exfoliation degree of the silicate layers in the PA-6 matrix. The amount of possible nucleating agents (individual layers or clay layer stacks) but also the amount of heterogeneities that retard the PA-6 crystal growth, increases with the exfoliation degree. The exfoliation degree in PA-6/MMT nanocomposites depends on the type of surfactants used to prepare the MMT layers and with the molecular weight of the PA-6 matrix. Dennis et al. found for PA-6 nanocomposites with Cloisite 15A and Cloistite 30B as MMT, that the exfoliation degree increased from 32 to 79 MMT particles per μm^2 [26]. Furthermore, Fornes et al. found for PA-6 nanocomposites with three different molecular weights of the polymer matrix, that the exfoliation degree in MMT particles per μm^2 increased from 92 at $M_n = 16{,}400$ g/mol, to 209 at $M_n = 22{,}000$ g/mol, and to 241 at $M_n = 29{,}300$ g/mol [27].

In this paper, the influence of the exfoliation degree on the crystallization behavior of polyamide-6/montmorillonite nanocomposites is further elaborated. Dynamic and isothermal differential scanning calorimetry (DSC) measurements were used to follow the crystallization in nanocomposites with three different types of MMT layers and three different molecular weight PA-6 grades. The polyamide-6/montmorillonite nanocomposites were further characterized by X-ray diffraction (XRD), transmission electron microscopy (TEM) and synchrotron small angle X-ray scattering (SAXS) measurements.

2. Experimental

2.1. Materials

Three types of virgin polyamide-6 (PA-6) of different molecular weight, Akulon K123 of $M_w = 25{,}000$ g/mol, Akulon K122 of $M_w = 22{,}000$ g/mol and Akulon K120 of $M_w = 18{,}500$ g/mol, were kindly supplied by DSM Engineering Plastics, Sittard, The Netherlands. These PA-6 types are referred to as PA-6k123, PA-6k122 and PA-6k120. montmorillonite types cloisite 15A (dimethyl bis(hydrogenated-tallow ammonium montmorillonite) and cloisite 30B (bis(2-hydroxyethyl) methyl tallow ammonium montmorillonite) were purchased from Southern Clay Products, Gonzales, USA. These MMT types are referred to as CL15A and CL30B. Montmorillonite type Nanomer I30Tc was purchased from Nanocor, Inc, Arlington Heights, USA, this MMT type is referred to as NaI30Tc.

Extruded PA-6 and the PA-6 nanocomposites were prepared under nitrogen atmosphere by melt-mixing in a co-rotating twin-screw mini-extruder at 260 °C for 15 min with a screw speed of 50 tours/min. Five series of PA-6 nanocomposites have been made. In the first three series, Akulon K123 was mixed with CL30B, NanomerI30Tc and CL15A, respectively. In the last two series, Akulon K122 and K120 were mixed with CL30B. The MMT loadings in all series were 1, 2, 4, 6, 8 and 10 wt%, respectively.

2.2. X-ray diffraction

XRD measurements were performed at room temperature using a Rigaku Kratky camera on a Rigaku Rotaflex RU-200B rotating Cu-anode at a power of 4 kW. No efforts were made to correct the patterns for smearing effects related to the use of a slit like source, as the evaluation is merely qualitative.

2.3. Transmission electron microscopy (TEM)

TEM micrographs were made on a Philips CM10, operating at 80 kV. Ultrathin sections were prepared on a Leica Ultracut ULT microtome, equipped with a Leica EM FCS cryo unit. The samples were trimmed with iron trimming knifes to trapezoidal shaped faces. Ultrathin sections (75 nm or less) were microtomed from these faces with a diamond knife (Drukker, International) at a sample temperature of −90 °C and with a knife temperature of −75 °C. The microtomed sections were collected in a water/dimethylsulfoxide (50/50) filled boat, attached to the diamond knife. The sections were collected out of the boat on copper TEM grids (square, 300 mesh) and dried completely on filter paper.

In order to quantify the degree of exfoliation, TEM micrographs of the nanocomposites have been used. For the quantification procedure the micrographs were printed on 21.6×27.9 cm^2 paper. The level of dispersion has been quantified in the following way. The number of particles in a section of the TEM micrographs was counted and divided by the area of this section. In this way, the mean TEM particle density (PD) can be determined. A particle has been defined as one individual silicate layer or as a silicate layer stack. The TEM particle density also depends on the MMT concentration. The TEM particle densities are therefore divided by the weight percent MMT to obtain the specific particle density (SPD). The specific TEM particle density, which is the average number of particles per μm^2 corrected for the MMT concentration of the nanocomposites, is therefore a measure of the extent of exfoliation. For the TEM micrographs, specific magnifications have been chosen to include a substantial number of platelets/agglomerates in order to improve the statistical validity of the analysis.

2.4. Differential scanning calorimetry (DSC)

DSC measurements were performed on a Perkin Elmer Pyris 1 DSC, calibrated with the melting point of indium (156.6 °C) and benzophenone (48.1 °C) for the temperature, and with indium (28.45 J/g) for the enthalpy. The block surrounding the measuring unit was thermostated at −30 °C with liquid nitrogen and the unit was flushed with dry nitrogen. All DSC curves are normalized to the sample mass (approximately 6 mg for a sample) and scanning rate after subtracting an empty pan measurement. As such pseudo-heat capacity data are obtained that have the units of specific heat capacity ($Jg^{-1}K^{-1}$) but that are not on an absolute scale [28].

The self-seeding experiments involve the following steps: (a) keeping the sample 5 min at 250 °C, (b) cooling at 10 °C/min down to 50 °C, (c) heating at 10 °C/min up to a given temperature T_{max}, waiting for 5 min at T_{max}, and finally (d) cooling at 10 °C/min down to 50 °C. The crystallization behavior in step (d) is evaluated as a function of T_{max}. The T_{max}'s used were 230, 235, 240, 250 and 280 °C.

The crystallization of the extruded samples was registered during cooling at 10 °C/min from 250 °C, or isothermally at 205 °C. Before cooling to room temperature or to 205 °C, the samples were kept at 250 °C for 5 min. For the calculation of the DSC crystallinities from the integrated exothermic peak areas, a value for the heat of fusion Δh_f of 237 J/g was taken [29].

2.5. Time-resolved small angle X-ray scattering (SAXS)

Time-resolved small-angle X-ray scattering (SAXS) experiments were conducted at the Dutch–Belgian Beamline (DUBBLE) at the European Synchrotron Radiation Facility (ESRF) in Grenoble, France. The wavelength of the incident X-rays was 1.2 Å. Powder data were collected on a 2D SAXS gas chamber wire detector at 2 m from the sample and in conjunction with a standard data acquisition system. The intensities were normalized to the intensity of the primary X-ray beam measured with an ionization chamber put upstream from the sample, corrected for the detector response and finally azimuthally averaged to yield 1D patterns. The scattering angles were calibrated using Silver Behenate.

Samples were mounted in copper holders. A Linkam hotstage was used for the temperature control of the samples. Samples were molten at a temperature of 250 °C for 5 min and then brought to the isothermal temperature of 205 °C. Data collection was started upon reaching 205 °C. Data were collected in subsequent time frames of 20 s until complete crystallization.

An averaged melt pattern was subtracted as a background from the SAXS patterns, collected over the angular range $0.0345 \leq s \leq 0.276\ nm^{-1}$ (with $s = 2\sin\theta/\lambda$, 2θ being the scattering angle and λ the wavelength). Details of this procedure have been described earlier in a paper dealing with PEO based nanocomposites [30] but it should be emphasized again that in this way the contribution to the scattering patterns by the nanocomposite morphology (i.e. the clay distribution) in the PA-6 matrix is effectively discarded. After a suitable extrapolation to zero and high angles linear correlation functions, $K(x)$ [31], were calculated by cosine transformation and processed as described earlier [30,32] yielding the long period, L_p, from the first side maximum in $K(x)$; the local volume fraction crystallinity in the PA-6 semicrystalline regions, ϕ_L, from the so-called quadratic expression; the crystalline lamellar thickness, l_c, and the amorphous lamellar thickness, l_a, from the product of L_p with ϕ_L or $(1-\phi_L)$, respectively. When using the quadratic expression independent information is needed to decide whether ϕ_L is associated with the minority or the majority fraction. Here the crystallinity values obtained from DSC are used as a guideline and ϕ_L was taken to be the minority phase over the full time range.

The volume fraction of semicrystalline regions, α_S, was calculated from the total scattering or invariant, Q_{id}, of the corresponding ideal two-phase structure, knowing the PA-6 crystalline, ρ_c, and amorphous, ρ_a, densities from the literature, ϕ_L and a scaling procedure [32]. For the crystalline and amorphous density, values of 1.23 and 1.08 g/cm^3 were taken, respectively [33]. In this procedure it was assumed that α_S equals one at complete crystallization (which is after 40 min isothermal crystallization in the case of the nanocomposites). The product $\alpha_S\phi_L$ is a measure for the overall volume fraction crystallinity (χ_v). Using the mass densities of the amorphous and crystalline phases, this volume fraction crystallinity was transformed into a mass fraction crystallinity χ_m for comparison with the DSC mass fraction crystallinity.

3. Results and discussion

3.1. Nanocomposite morphology

Figs. 1–5 show the XRD patterns of the PA-6k123/CL30B, PA6k123/NaI30Tc, PA-6k123/CL15A, PA-6k122/CL30B and PA-6k120/CL30B nanocomposites, respectively. For a given polymer/clay combination the patterns of pure polymer and pure MMT are collected in one figure together with nanocomposites with different MMT contents. The curves

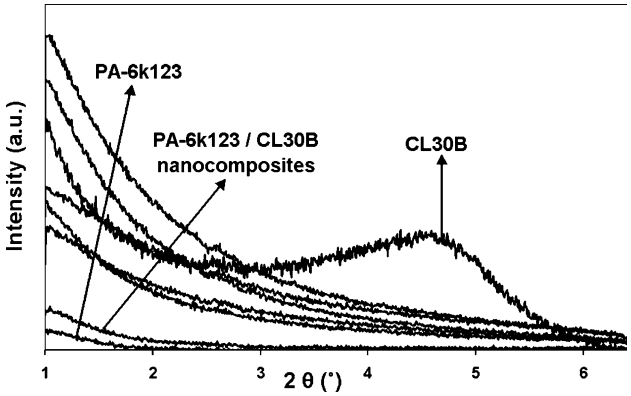

Fig. 1. XRD-patterns of PA-6k123, CL30B and the PA-6k123/CL30B nanocomposites. The patterns are shifted vertically for clarity. The mostdown pattern refers to the pure polymer and MMT content increases with intensity from 1 to 10 wt%.

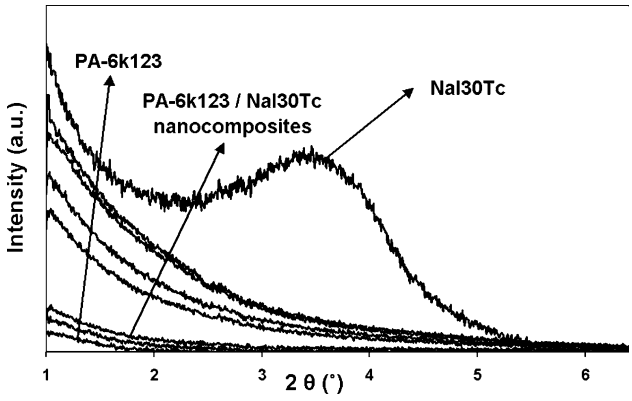

Fig. 2. XRD-patterns of PA-6k123, NaI30Tc and the PA-6k123/NaI30Tc nanocomposites. The patterns are shifted vertically for clarity. The mostdown pattern refers to the pure polymer and MMT content increases with intensity from 1 to 10 wt%.

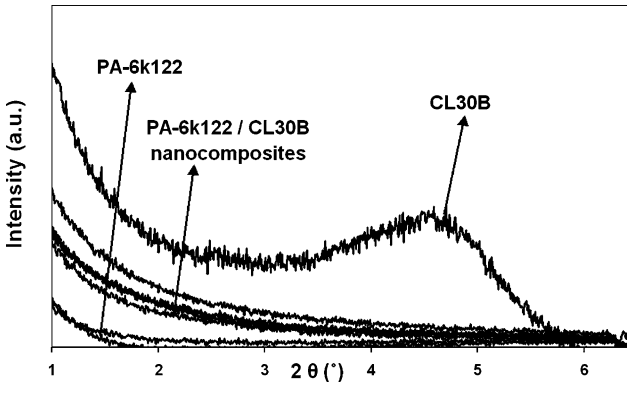

Fig. 4. XRD-patterns of PA-6k122, CL30B and the PA-6k122/CL30B nanocomposites. The patterns are shifted vertically for clarity. The mostdown pattern refers to the pure polymer and MMT content increases with intensity from 1 to 10 wt%.

related to the different nanocomposites are not labeled but they can easily be identified as the intensities of the patterns at the lowest angles increase with increasing MMT content. The XRD patterns of CL30B, NaI30Tc and CL15A display diffraction peaks at $2\theta = 4.8°$, $2\theta = 3.5°$ and $2\theta = 2.3°$, which correspond to silicate interlayer distances of 18, 25 and 38 Å, respectively. The patterns of PA-6k123/CL30B, PA6k123/NaI30Tc, PA-6k122/CL30B and PA-6k120/CL30B nanocomposites show no MMT diffraction peaks, which indicates an exfoliated dispersion of the silicate layers in the polymer matrix. Such a peak is only present in the case of PA6k123/CL15A nanocomposites (Fig. 3) and moreover at the same diffraction angle as pure CL15A, i.e. at $2\theta = 2.3°$, indicating the total absence of intercalation. Whether or not these systems are partially exfoliated cannot be decided from the XRD patterns.

TEM micrographs of all PA-6k123/CL30B, PA6k123/NaI30Tc, PA-6k123/CL15A, PA-6k122/CL30B and PA-6k120/CL30B nanocomposites have been made. One representative for each of these compositions is shown in Fig. 6. The TEM micrographs of the PA-6k123/CL30B, PA6k123/NaI30Tc, PA-6k122/CL30B and PA-6k120/CL30B nanocomposites confirm the XRD observations. These nanocomposites all have a highly exfoliated nanomorphology; the micrographs almost exclusively show very thin black lines, associated with individual silicate layers. Only very occasionally slightly thicker black lines can be found that may point at silicate layer stacks. In contrast, a high amount of silicate layer stacks is present in the PA-6/CL15A nanocomposites (Fig. 6(c)), which is in agreement with the presence of a peak in XRD. However, some individual silicate layers are present also, which means that the PA-6/CL15A nanocomposites posses a partially intercalated/exfoliated morphology. Only the PA-6/CL15A nanocomposites possess a partially exfoliated nanomorphology. The diffraction peaks that were found for these nanocomposites in XRD originate from the non-exfoliated silicate layer stacks.

In order to quantify the degree of exfoliation of the PA-6 nanocomposites image analysis has been performed on all TEM micrographs and a specific particle density (SPD) has been calculated for all PA-6 nanocomposites. The specific TEM particle density is the average number of particles per μm^2 corrected for the MMT concentration of the nanocomposites.

The SPD's for PA-6k123/MMT nanocomposites with different types of montmorillonite are depicted in Fig. 7.

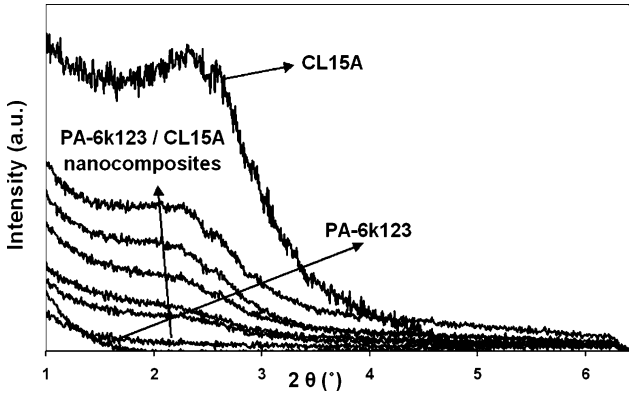

Fig. 3. XRD-patterns of PA-6k123, CL15A and the PA-6k123/CL15A nanocomposites. The patterns are shifted vertically for clarity. The mostdown pattern refers to the pure polymer and MMT content increases with intensity from 1 to 10 wt%.

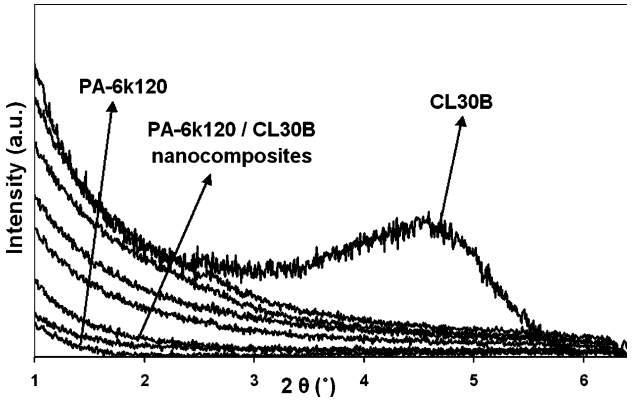

Fig. 5. XRD-patterns of PA-6k120, CL30B and the PA-6k120/CL30B nanocomposites. The patterns are shifted vertically for clarity. The mostdown pattern refers to the pure polymer and MMT content increases with intensity from 1 to 10 wt%.

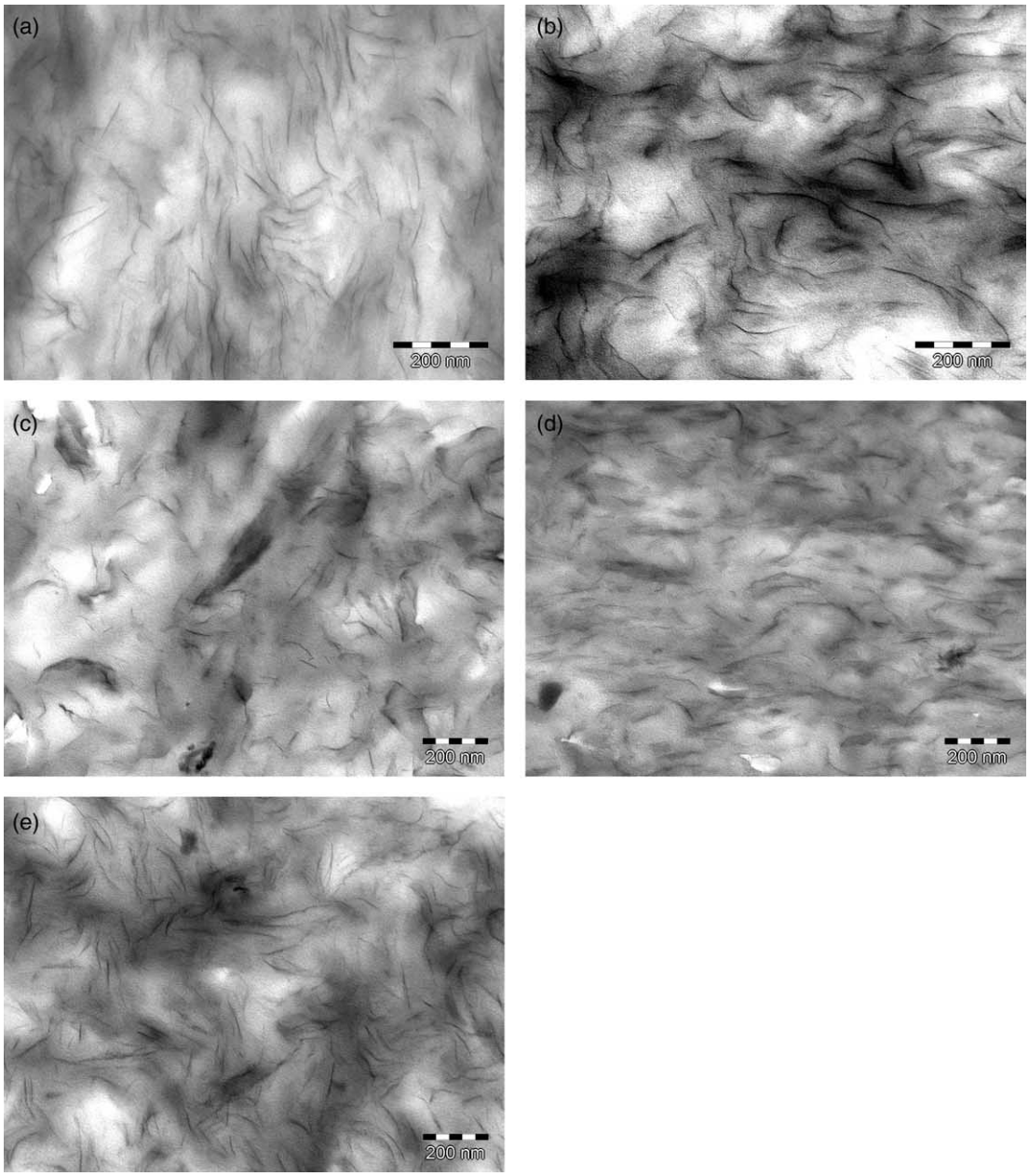

Fig. 6. TEM micrographs of PA-6k123 + 6 wt% CL30B (a), PA-6k123 + 6 wt% NaI30Tc (b), PA-6k123 + 6 wt% CL15A (c) PA-6k122 + 6 wt% CL30B (d) and PA-6k120 + 6 wt% CL30B (e), respectively.

The exfoliation degrees of PA-6k123/CL30B nanocomposites are slightly higher than those of PA-6k123/NaI30Tc nanocomposites. The exfoliation degree of PA-6k123/CL15A nanocomposites is much lower than that of the other two PA-6k123/MMT nanocomposites. Furthermore, the SPD decreases with increasing MMT concentration; in other words, the degree of exfoliation decreases with increasing MMT concentration. When the MMT concentration is increased, the silicate layer stacks are less and less able to exfoliate, and more and more silicate layer stacks remain in the final nanocomposite.

The SPD's for PA-6/CL30B nanocomposites with different matrix molecular weights are depicted in Fig. 8. The exfoliation degrees of PA-6k123/CL30B nanocomposites are higher than those of PA-6k122/CL30B nanocomposites, and the latter are higher than those of PA-6k120/CL30B nanocomposites. The SPD of the PA-6k120/CL30B nanocomposites also decreases slightly with increasing MMT concentration.

3.2. The influence of melt-extrusion on the nucleation behavior of polyamide-6

As described in the introduction, the crystallization temperature of PA-6 increases with about 15 °C upon melt-extrusion. It has been suggested that partly oriented segments of polymer chains that are generated during extrusion are transformed into efficient and stable nucleating agents upon

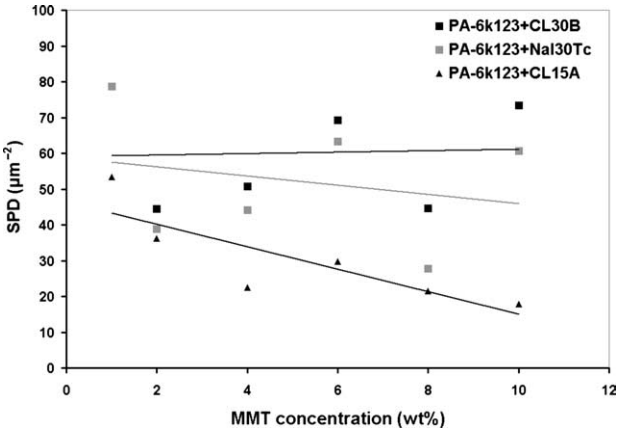

Fig. 7. Specific particle density (SPD) for PA-6k123/MMT nanocomposites with different types of montmorillonite.

cooling [10,22–25]. An attempt is made below to quantify this change in nucleating efficiency.

A substance can facilitate polymer nucleation easily in case there is some crystal lattice matching between the lattice of the nucleating agent and that of the crystalline polymer. Such a match is obvious for crystals of the polymer itself. As a result, nucleation is most efficient in a self-seeding experiment where due to incomplete melting some crystal residues are left in the melt that nucleate crystallization in a subsequent cooling run [28,34]. Fillon et al. defined the nucleation efficiency, NE, of a given substance by the following ratio [34]:

$$\mathrm{NE} = 100\,\frac{T_{\mathrm{cNA}} - T_{\mathrm{c1}}}{T_{\mathrm{c2max}} - T_{\mathrm{c1}}} \tag{1}$$

The NE is expressed as a percentage between 0 and 100, where 0 stands for no nucleation action and 100 for optimum efficiency. T_{c1} represents the crystallization peak temperature of the polymer to which no nucleating substances are added, T_{c2max} is the crystallization peak temperature of the same virgin polymer but self-nucleated to saturation and T_{cNA} is the crystallization peak temperature of the polymer to which a nucleating agent was added.

Fig. 9 illustrates the crystallization behavior of the virgin and extruded PA-6 sample as a function of T_{max}. Clearly, the crystallization peak and onset temperatures of the virgin samples (thick lines) shift to higher temperatures with decreasing T_{max} due to incomplete melting and hence self-nucleation. In principle, self-seeding is possible when samples are not heated above the equilibrium melting temperature, which is 260 °C for PA-6 according to the ATHAS databank [29]. However, in the present case all crystallization curves recorded during cooling from temperatures $T_{\mathrm{max}} > 250$ °C are identical, pointing at the absence of any left crystal residues at and above 250 °C. The crystallization peak during cooling from 250 °C occurs at 171.5 °C and represents T_{c1}. Here the peak temperature during cooling from 230 °C represents T_{c2max} and occurs at 189.5 °C. The crystallization peak of the extruded sample cooled from 250 °C occurs at 187.5 °C (T_{cNA}), which results in an exceptionally high NE after extrusion of 89% (the best nucleation agents for, e.g. isotactic polypropylene only rate at 66% [34]). Hence, the actual nucleation efficiency of the extrusion-induced structures is probably as high as that of the crystal residues in a self-seeding experiment, implying that the NE value differs from 100% only because the number of nuclei in the extruded sample is below that of the 'to saturation self-nucleated' sample. The crystallization peaks of the extruded sample do hardly depend on T_{max}. A minor shift (2 °C) to a higher temperature is only observed for $T_{\mathrm{max}} = 230$ °C, with a peak at 189.5 °C, due to an increased number of nuclei by self-seeding. Here the NE value nearly equals 100% (actually 98%). Apparently, the oriented segments of polymer chains that are generated during extrusion are transformed into nucleating structures upon cooling that are very efficient nucleating agents.

Therefore, it can be expected that the role of silicate layers as nucleating agents in PA-6 nanocomposites that have been made by melt-extrusion is insignificant because such samples already contain an increased amount of extrusion induced nuclei.

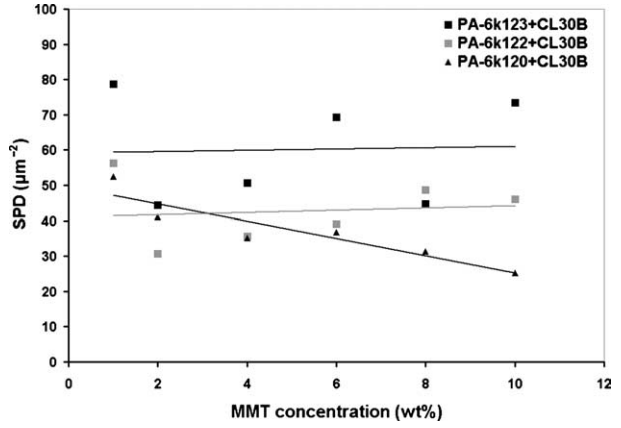

Fig. 8. Specific particle density (SPD) for PA-6/CL30B nanocomposites with different matrix molecular weights.

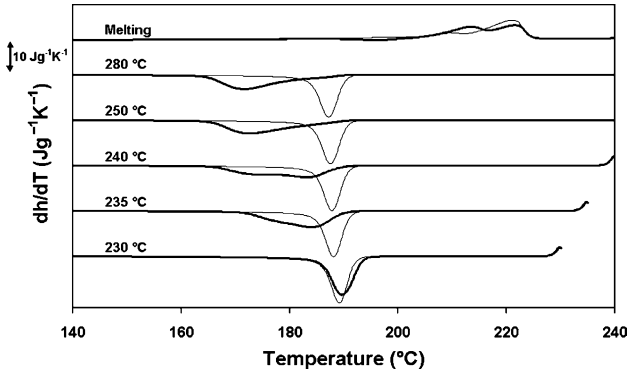

Fig. 9. DSC curves recorded during cooling from the indicated (T_{max}) temperatures for virgin (thick lines) and extruded PA-6 (thin lines). Melting curves after cooling from 250 °C are added for a better appreciation of the selected T_{max}. Scan rates 10 °C/min.

3.3. The crystallization behavior of PA-6/montmorillonite nanocomposites

The DSC crystallization behavior during cooling (a) and isothermally at 205 °C (b) for extruded pure PA-6k123 and for extruded PA-6k123/CL30B nanocomposites is shown in Fig. 10. The crystallization onset and peak temperatures decrease considerably with increasing MMT content (approximately 8 °C from pure PA-6k123 to PA-6k123 + 10% CL30B) and the peak width concomitantly increases. Clearly, the overall crystallization rate decreases when MMT silicate layers are added. Similarly, in the curves associated with isothermal crystallization (Fig. 10(b)), the crystallization onset and half-times increase with increasing MMT content. Furthermore, the overall crystallization time, proportional to the crystallization peak width, increases tremendously with increasing MMT content (from 15 to almost 80 min).

In these crystallization experiments, the silicate layers have a strong retarding effect on PA-6 crystal growth. In the crystallization of PA-6, the silicate layers are thought to hinder the diffusion of polymer chains towards the crystal growth front. The silicate layers behave like impurities that have to migrate away from the crystallization front, which takes time. Alternatively, if migration would not be possible, the crystallization front when it collides with an MMT platelet has to change its direction or can even be stopped from growing further. The retarding effect of the silicate layers on PA-6 crystal growth increases with increasing MMT content, obviously because the probability of a collision increases. In other words, the pathlength along which crystals are free to grow reduces as the interparticle distance between the silicate layers progressively decreases.

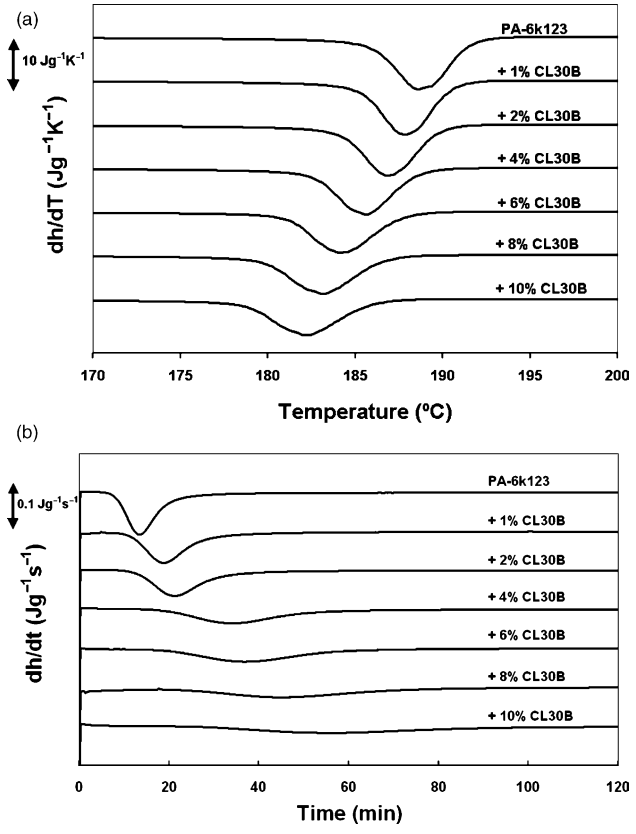

Fig. 10. DSC cooling curves at 10 °C/min (a) and isothermal crystallization at 205 °C (b) of extruded PA-6k123 and PA-6k123/Cl30B nanocomposites. The curves have been shifted vertically for clarity. The endothermic heat flow rate points upwards.

In the studied PA-6k123/CL30B nanocomposites, the retarding effect of the silicate layers is so strong that no nucleating activity at lower MMT concentration can be observed. This strong effect is the result of the high exfoliation degree of the PA-6k123/CL30B nanocomposites (Figs. 1 and 6(a)). These nanocomposites contain therefore very high amounts of individual silicate layers that act as retarding impurities to the crystallization of PA-6. Moreover, the absence of any obvious nucleating power of the silicate layers is also caused by the predominant nucleation enhancement after preparing PA-6 via melt-extrusion, as described in Section 3.2. Furthermore, in principle one cannot enhance primary nucleation limitless by the addition of more and more nucleators. The most active sites will trigger crystallization, leaving less active sites unused. So therefore, the relative effect of adding nucleating agents decreases with increasing MMT concentrations.

3.4. The influence of montmorillonite type on the crystallization behavior of PA-6/montmorillonite nanocomposites

The crystallization behavior of PA-6 nanocomposites with three different montmorillonite types is compared in this section, namely the PA-6k123/CL30B, PA-6k123/NaI30Tc and PA-6k123/CL15A nanocomposites. The crystallization behavior of the PA-6k123/CL30B nanocomposites with increasing CL30B content has already been described in the previous section.

Most important in this discussion are the evolution of the crystallization peak temperature during cooling at 10 °C/min and the crystallization half time during isothermal crystallization at 205 °C. An overview of the crystallization peak-temperatures during cooling at 10 °C/min and the crystallization half-times of the isothermal measurements at 205 °C of all the three PA-6 nanocomposites series with each a different montmorillonite type, is depicted in Fig. 11(a) and (b).

Clearly, the crystallization rates decrease with increasing MMT content for the PA-6k123/CL30B nanocomposites, and a bit less pronounced for the PA-6k123/NaI30Tc nanocomposites. On the contrary, the PA-6k123/CL15A crystallization kinetics are slightly enhanced with increasing MMT content. It is known from the XRD and TEM measurements, described in Section 3.1, that PA-6k123/CL30B and PA-6k123/NaI30Tc nanocomposites exhibit a highly exfoliated nanomorphology while the PA-6k123/CL15A nanocomposites have a poorly exfoliated morphology with an abundance of clay stacks that are not different from the original ones prior to melt mixing. Comparison of the TEM micrographs of the PA-6k123/CL30B and PA-6k123/NaI30Tc nanocomposites (Fig. 6(a) and (b)) with those of the PA-6k123/CL15A nanocomposites in Fig. 6(c) clearly shows that the interparticle distance between

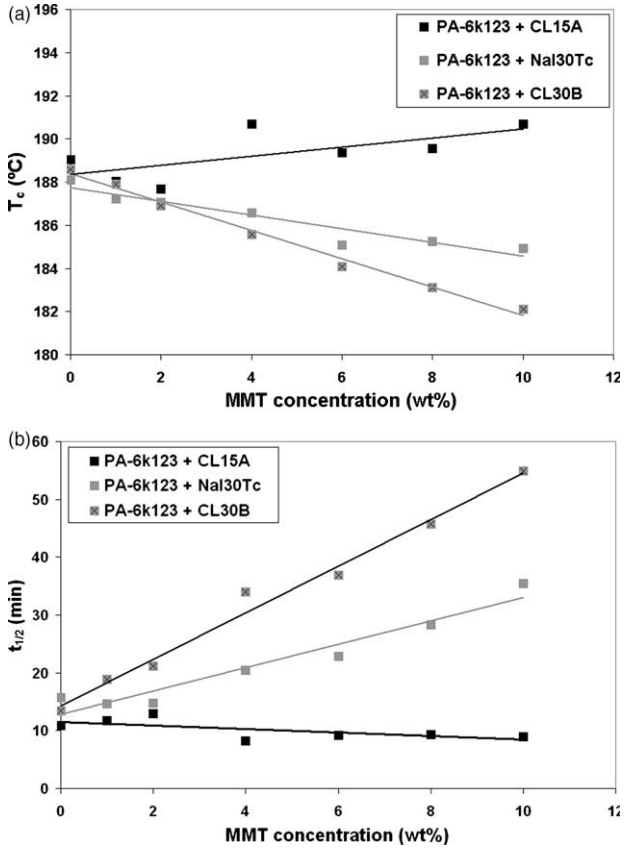

Fig. 11. Overview of the crystallization results by DSC of PA-6k123/CL30B, PA-6k123/NaI30Tc and PA-6k123/CL15A nanocomposites. Peak-temperatures of the cooling curves at 10 °C/min are depicted in (a) and half-times of crystallization of the isothermal measurements at 205 °C in (b).

the silicate entities (being individual layers or stacks) is smaller for the PA-6k123/CL30B and PA-6k123/NaI30Tc nanocomposites compared to the PA-6k123/CL15A nanocomposites. Also, the specific particle densities (SPD) that were determined in Section 3.1 clearly show that the degree of exfoliation of the PA-6k123/CL30B and PA-6k123/NaI30Tc nanocomposites is much higher than those of the PA-6k123/CL15A nanocomposites. These nanocomposites therefore possess a smaller interparticle distances at a given concentration. The observations on PA-6k123/CL30B and PA-6k123/CL15A nanocomposites are in agreement with those reported by Dennis et al. [26]. The substantial amount of individual layers in the PA-6k123/CL15A nanocomposites does not give rise to any retarding impurity effect on the crystallization behavior of the PA-6 matrix, pointing at a very delicate balance between nucleation enhancement on the one hand and growth retardation on the other hand. A small shift in exfoliation degree of the silicate layers in the PA-6 nanocomposites, shifts the balance to either nucleation or growth retardation with accordingly strong changes to the PA-6 crystallization behavior in these composite series. Comparison of the crystallization behavior of PA-6k123/CL30B with that of the PA-6k123/NaI30Tc nanocomposites also points to the importance of slight differences in exfoliation degree. The crystallization rates of both the PA-6k123/CL30B and PA-6k123/NaI30Tc nanocomposites decrease with increasing MMT content, but this decrease is stronger for the PA-6k123/CL30B nanocomposites although TEM only reveals slight differences in exfoliation degree. Very small differences in silicate layer morphology can thus have a profound effect on the crystallization behavior of the PA-6 matrix.

3.5. The influence of matrix molecular weight on the crystallization behavior of PA-6/montmorillonite nanocomposites

The crystallization behavior of PA-6 nanocomposites with three different matrix molecular weights is compared in this section, namely the PA-6k123/CL30B, PA-6k122/CL30B and PA-6k120/CL30B nanocomposites. The crystallization behavior of the PA-6k123/CL30B nanocomposites was already described in Section 3.3.

Again, most important in this discussion are the evolution of the crystallization peak temperature during cooling at 10 °C/min and the crystallization half time during isothermal crystallization at 205 °C. An overview of peak-temperatures and half-times of the three PA-6 nanocomposites series with each a different molecular weight, is depicted in Fig. 12(a) and (b).

During isothermal crystallization at 205 °C (Fig. 12(b)) only a decrease of the crystallization rate can be observed with

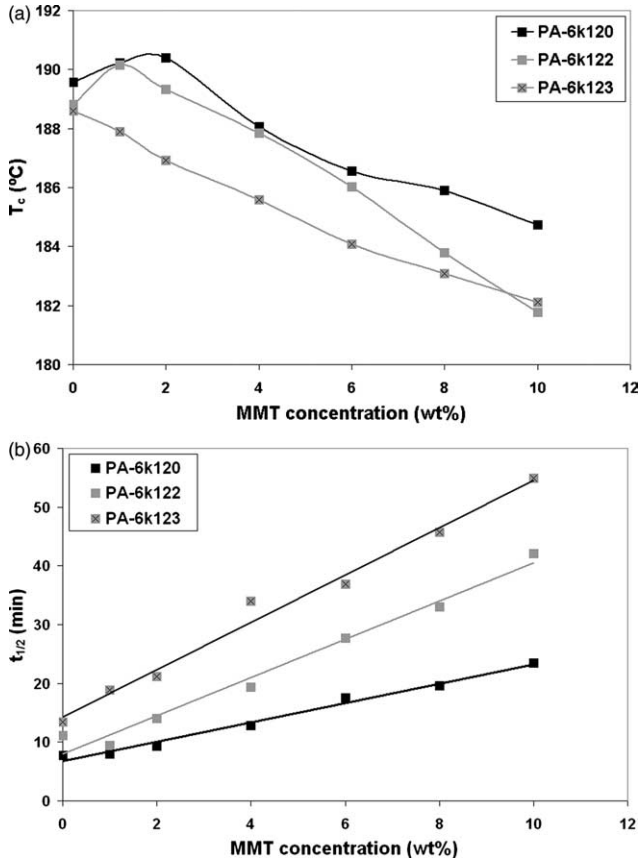

Fig. 12. Overview of the crystallization results by DSC of PA-6k123/CL30B, PA-6k122/CL30B and PA-6k120/CL30B nanocomposites. Peak-temperatures of the cooling curves at 10 °C/min are depicted in (a) and half-times of the isothermal measurements at 205 °C in (b).

increasing MMT content, to an extent (slope) proportional to the molecular weight. The XRD and TEM measurements, described in Section 3.1, only point at minor differences in nanomorphology between these PA-6/CL30B nanocomposites with respect to the difference in matrix molecular weight. All nanocomposites exhibit a highly exfoliated nanomorphology (Fig. 6(a), (d) and (e)). The specific particle densities (SPD) that were determined in Section 3.1 clearly show that the exfoliation degrees of PA-6k123/CL30B nanocomposites are higher than those of PA-6k122/CL30B nanocomposites, and the latter are higher than those of PA-6k120/CL30B nanocomposites. The interparticle distance between the silicate entities (being individual layers or stacks) at a given concentration, therefore decreases from PA-6k123/CL30B (higher M_w) to PA-6k120/CL30B (lower M_w) nanocomposites. Furthermore, it is known that the degree of exfoliation of silicate layers increases with increasing matrix molecular weight due to the presence of higher shear forces during melt mixing [27]. The interparticle distance between the silicate layers decreases only slightly with increasing PA-6 molecular weight but apparently, these small differences are sufficient to result in significant changes in crystallization behavior.

The evolution of the crystallization peak temperatures in Fig. 12(a) qualitatively follows the retardation trend found in Fig. 12(b), except that the low molar mass matrices display an enhanced crystallization rate (i.e. earlier or here: at higher temperature) when the MMT amount is low. Enhanced crystallization points at promoted nucleation and it only seems to be visible when the retarding effect does not dominate. The retarding effect dominates in the case of PA-6K123 that has the highest degree of exfoliation, hence the highest number of particles and hence the lowest interparticle distance.

The question now arises why this nucleating effect does not show up at a lower degree of supercooling, i.e. during isothermal crystallization at 205 °C. Apparently, one has to accept that a larger degree of supercooling is needed for the silicate layers to become active as nucleators. In this view also the increase of the crystallization peak temperature for the PA-6k123/CL15A with increasing MMT amount (Fig. 11(a)) can be explained as well as the absence of such an effect at lower supercooling during isothermal crystallization (Fig. 11(b)). It has to be noted that in the case of PCL intercalated nanocomposites the nucleating ability persisted at two different degrees of supercooling, but that the retarding effect disappeared at low supercooling [35]. The latter effect was attributed to the slow crystal growth rate compared to the migration rate of the impurities at low supercooling by which the latter are de facto no longer acting as disturbing entities. Such an effect is less probable in the present PA-6 case where the amount of particles (by full exfoliation) is too high to be effectively circumvented.

3.6. The lamellar structure of PA-6k123 and PA-6k123/CL30B nanocomposites

The influence of the silicate layers on the lamellar morphology of the PA-6 crystalline phase in the nanocomposites is highlighted in this section. The long periods, crystalline and amorphous lamellar thicknesses and SAXS overall crystallinities were determined for pure PA-6 and the PA-6k123/CL30B nanocomposites as a function of time with real-time synchrotron SAXS during isothermal crystallization at 205 °C but since no evolution could be observed during the course of crystallization, averaged parameters are given in Table 1. The absence of any evolution in these parameters points at the absence of secondary crystallization in terms of lamellar insertion or thickening. Note that only the results for PA-6k123 and the PA-6/CL30B nanocomposites with 1,2,4 and 6 wt% of CL30B are given. The MMT background is too dominant in the SAXS patterns of the PA-6k123 + 8% CL30B and PA-6k123 + 10% CL30B nanocomposites and could not properly be discarded. Therefore these are not considered here.

Considering the statistical fluctuation in the data, the long periods, crystalline and amorphous layer thicknesses and SAXS crystallinities are similar for pure PA-6k123 and all the PA-6k123/CL30B nanocomposites. So, there are no major changes in the lamellar texture of the PA-6 matrix caused by the incorporation of silicate layers and the disturbed crystal growth does not result in major changes in the lamellar stack morphology. The SAXS overall crystallinities are considerably higher than the DSC crystallinities, which can be due to the contribution in SAXS of crystalline-amorphous transition layers [36] or dense rigid amorphous material in between the lamellar crystal grains [37]. However, the SAXS overall mass fraction crystallinities depicted in Table 1 are close enough to

Table 1
Long period, crystalline and amorphous lamellar thickness and mass fraction crystallinity of PA-6k123 and PA-6k123/CL30B nanocomposites, calculated from the synchrotron SAXS measurements during isothermal crystallization at 205 °C

Material	L_P (Å)	l_c (Å)	l_a (Å)	SAXS crystallinity (%)	DSC crystallinity (%)
PA-6k123	128 ± 4	39 ± 1	89 ± 4	33 ± 1	25 ± 2
PA-6k123 + 1% CL30B	136 ± 4	45 ± 1	91 ± 4	36 ± 1	23 ± 2
PA-6k123 + 2% CL30B	133 ± 4	45 ± 2	88 ± 5	37 ± 1	24 ± 2
PA-6k123 + 4% CL30B	136 ± 3	46 ± 2	90 ± 3	37 ± 1	24 ± 2
PA-6k123 + 6% CL30B	135 ± 9	42 ± 3	93 ± 10	34 ± 1	23 ± 2

The mass fraction crystallinity obtained from DSC measurements is added for comparison.

those of DSC to justify the assumption that ϕ_L is associated with the minority component (see Section 2).

4. Conclusions

The PA-6k123/CL30B, PA6k123/NaI30Tc, PA-6k122/CL30B and PA-6k120/CL30B nanocomposites exhibit a highly exfoliated nanomorphology in which the MMT is mostly present as individual silicate layers. Only the PA-6/CL15A nanocomposites possess a partially exfoliated nanomorphology; with a dominant presence of unmodified MMT silicate stacks.

The silicate layer nucleating power is poor in PA-6 nanocomposites made by melt-extrusion because of melt-processing induced PA-6 typical nuclei. In most melt-extruded PA-6/MMT nanocomposites the dispersed silicate layers decrease rather than increase the PA-6 crystallization rate, especially at high MMT contents since the silicate layers hinder the diffusion of polymer chains to the crystal growth front and since impurity migration away from the growth front takes time. For a given amount of MMT this effect increases with increasing degree of exfoliation, which dependents on the MMT type and which increases with increasing PA-6 molecular weight. However, such a retarding effect is absent with the MMT type that resulted in a poorly exfoliated nanomorphology. The disturbed crystal growth does not result in major changes in the PA-6 semicrystalline stack morphology.

Moderate nucleation effects due to the presence of MMT can be observed when the particle load is low (low amount of MMT and/or poor degree of exfoliation) and provided the supercooling is sufficiently large.

Acknowledgements

The authors would like to thank the Fund for Scientific Research, Flanders (Belgium) as well as the Research Council KULeuven for the financial support of this research; one of them (B.G.) is a postdoctoral fellow of the Fund for Scientific Research, Flanders. The authors also would like to acknowledge the Dutch–Belgian beamline (DUBBLE) research group at the ESRF, Grenoble, France, for their help and support with the time-resolved small angle X-ray experiments.

References

[1] Alexandre M, Dubois P. Mater Sci Eng 2000;28(1–2):1–63.
[2] Giannelis EP, Krishnamoorti R, Manias E. Adv Polym Sci 1999;138:107–47.
[3] Lincoln DM, Vaia RA, Wang Z-G, Hsiao BS. Polymer 2001;42:1621–31.
[4] Lepoittevin B, Devalckenaere M, Pantoustier N, Alexandre M, Kubies D, Calberg C, et al. Polymer 2002;43(14):4017–23.
[5] Pantoustier N, Lepoittevin B, Alexandre M, Kubies D, Calberg C, Jerome R, et al. Polym Eng Sci 2002;42(9):1928–37.
[6] Maiti P, Nam PH, Okamoto M, Hasegawa N, Usuki A. Macromolecules 2002;35:2042–9.
[7] Moussaif N, Groeninckx G. Polymer 2003;44:7899–906.
[8] Groeninckx G, Berghmans H, Overbergh N, Smets G. J Polym Sci, Polym Phys Ed 1974;12:303–16.
[9] Wunderlich B. Macromolecular physics. vol. 2. New York: Academic Press; 1976 [chapter 5].
[10] Fornes TD, Paul DR. Polymer 2003;44:3945–61.
[11] Wu TM, Chen EC. Polym Eng Sci 2002;42(6):1141–9.
[12] Wu TM, Wu JY. J Macromol Sci Phys 2002;B41(1):17–31.
[13] Maiti P, Nam PH, Okamoto M, Kotaka T. Polym Eng Sci 2002;42(9):1864–71.
[14] Kamal MR, Borse NK, Garcia-Rejon A. Polym Eng Sci 2002;42(9):1883–96.
[15] Liu X, Wu Q. Polymer 2002;43:1933–6.
[16] Liu X, Wu Q. Eur Polym J 2002;38:1383–9.
[17] Medellin-Rodriguez FJ, Burger C, Hsiao BS, Chu B, Vaia RA, Phillips S. Polymer 2001;42:9015–23.
[18] Priya L, Jog JP. J Polym Sci, Part B: Polym Phys 2002;40:1682–9.
[19] Lincoln DM, Vaia RA, Wang ZG, Hsiao BS, Krishnamoorti R. Polymer 2001;42:9975–85.
[20] Xu W, Ge M, He P. J Polym Sci, Part B: Polym Phys 2002;40:408–14.
[21] Van Es M. Polymer-clay nanocomposites, PhD Thesis, Technical University of Delft, The Netherlands: ISBN 90 77017 27 5, 2001 [chapter 7].
[22] Vieweg/Müller, Kunststoff Handbuch band VI, Polyamide, Carl Hanser Verlag, München, 1966, 449–455.
[23] Khanna YP, Reimschuessel AC, Banerjie A, Altman C. Polym Eng Sci 1988;28(24):1600–6.
[24] Khanna YP, Kumar R. Reimschuessel Polym Eng Sci 1988;28(24):1607–11.
[25] Tidick P, Fakirov S, Avramova N, Zachmann HG. Colloid Polym Sci 1984;262:445–9.
[26] Dennis HR, Hunter DL, Chang D, Kim S, White JL, Cho JW, et al. Polymer 2001;42:9513–22.
[27] Fornes TD, Yoon PJ, Keskkula H, Paul DR. Polymer 2001;42:9929–40.
[28] Mathot VBF. Calorimetry and thermal analysis of polymers. New York: Hanser Publishers; 1994 [(a) Chapter 5, p. 105; (b) Chapter 9, p. 231].
[29] Athas Databank, URL: http://web.utk.edu/~athas/databank/Intro.Html, last revision February 5; 2000.
[30] Homminga DS, Goderis B, Reynaers H, Groeninckx G. Polymer 2005;46(23):9941-9954.
[31] Strobl GR, Schneider M. J Polym Sci, Polym Phys Ed 1980;18:1343–59.
[32] Goderis B, Reynaers H, Koch MHJ, Mathot VBFJ. Polym Sci, Part B: Polym Phys 1999;37:1715–38.
[33] Brandrup J, Immergut EH. Polymer handbook. 3rd ed. New York: Wiley; 1989 [chapter 6].
[34] Fillon B, Lotz B, Thierry A, Wittmann JC. J Polym Sci, Part B: Polym Phys 1993;31(10):1395–405.
[35] Homminga D, Goderis B, Dolbnya I, Reynaers H, Groeninckx G. Crystallization behavior of polymer/montmorillonite nanocomposites. Part II. Intercalated poly(ε-caprolactone)/montmorillonite nanocomposites. Polymer 2005, submitted.
[36] Goderis B, Reynaers H, Koch MHJ. Macromolecules 2002;35(15):5840–53.
[37] Goderis B, Klein PG, Hill SP, Koning CE. Prog. Colloid Polym. Sci. 2005;130:1-11.